

**Carrier tuning of Stoner ferromagnetism in ThCr<sub>2</sub>Si<sub>2</sub>-structure cobalt arsenides**B. G. Ueland <sup>1,2,\*</sup> Santanu Pakhira <sup>1,2</sup> Bing Li <sup>1,2</sup> A. Sapkota <sup>1,2,†</sup> N. S. Sangeetha <sup>1,‡</sup>  
T. G. Perring,<sup>3</sup> Y. Lee,<sup>1</sup> Liqin Ke,<sup>1</sup> D. C. Johnston <sup>1,2</sup> and R. J. McQueeney<sup>1,2,§</sup><sup>1</sup>Ames Laboratory, U.S. DOE, Iowa State University, Ames, Iowa 50011, USA<sup>2</sup>Department of Physics and Astronomy, Iowa State University, Ames, Iowa 50011, USA<sup>3</sup>ISIS Neutron and Muon Source, STFC Rutherford Appleton Laboratory, Didcot, Oxon OX11 0QX, United Kingdom

(Received 9 March 2021; accepted 7 December 2021; published 27 December 2021)

CaCo<sub>2-y</sub>As<sub>2</sub> is an unusual itinerant magnet with signatures of extreme magnetic frustration. The conditions for establishing magnetic order in such itinerant frustrated magnets, either by reducing frustration or increasing electronic correlations, is an open question. Here, we use results from inelastic neutron scattering and magnetic susceptibility measurements and density functional theory calculations to show that hole doping in Ca(Co<sub>1-x</sub>Fe<sub>x</sub>)<sub>2-y</sub>As<sub>2</sub> suppresses magnetic order by quenching the magnetic moment while maintaining the same level of magnetic frustration. The suppression is due to tuning the Fermi energy away from a peak in the electronic density of states originating from a flat conduction band. This results in the complete elimination of the magnetic moment by  $x \approx 0.25$ , providing a clear example of a Stoner-type transition.

DOI: [10.1103/PhysRevB.104.L220410](https://doi.org/10.1103/PhysRevB.104.L220410)

Iron and cobalt pnictide metals harbor weak to moderate magnetism driven by features in their electronic-band structure lying close to the Fermi energy  $E_F$ . Tuning the chemical composition of such materials has resulted in intriguing properties related to the underlying magnetism including non-Fermi-liquid behavior [1], magnetic glassiness [2], electronic nematicity [3], and unconventional superconductivity [4–6]. While often discussed using a local-moment description [7–9], it is clear that the itinerant nature of the magnetism in these compounds is essential for facilitating the tunability of these phenomena. More generally, compared to our knowledge of local-moment magnetism, our understanding of itinerant magnetism is limited by the relatively poorer experimental representation of purely itinerant-moment systems [10]. In this Letter, we report the direct observation of quenching of the magnetic moment in a Co pnictide by a Stoner-type transition [11].

The ThCr<sub>2</sub>Si<sub>2</sub>-type (122) pnictide CaCo<sub>2-y</sub>As<sub>2</sub>, where  $y$  corresponds to vacancies on the Co site, has the crystal structure shown in Fig. 1(a) [12,13] which is closely matched to the Fe-pnictide superconductors [7,14–16]. Contemporary studies of CaCo<sub>2-y</sub>As<sub>2</sub> were initially aimed at discovering the conditions necessary to create a superconducting state similar to that found in the Fe-based pnictides. However, its A-type antiferromagnetic (AFM) order [shown in Fig. 1(a)] was found to be quite intriguing, exhibiting ferromagnetic (FM) Co layers

with evidence for extreme magnetic frustration [8,17] and signatures of itinerant magnetism [12,18–20].

Extreme frustration was found in CaCo<sub>1.86</sub>As<sub>2</sub> via inelastic neutron scattering (INS) measurements made below the Néel temperature of  $T_N = 52(1)$  K [12,19,20]. These data show quasi-one-dimensional (1D) spin fluctuations dominated by the FM Co layers instead of well-defined spin waves [8]. As explained below, describing this behavior using a local-moment (Heisenberg) model places the compound at the border between FM and stripe-AFM ordering which indicates extreme frustration. On the other hand, CaCo<sub>1.86</sub>As<sub>2</sub> exhibits a weak ordered magnetic moment of  $\mu = 0.80(9)\mu_B/\text{f.u.}$  [20], temperature-independent contributions to the magnetic susceptibility  $\chi$ , and a somewhat large Sommerfeld coefficient of  $\gamma = 27(1)$  mJ/mol K<sup>2</sup> [19] which all point to its magnetism being itinerant.

In general, frustrated and itinerant magnetic systems each have different conditions for establishing magnetic order. In the former case, some relief from frustration, for example, by modifications of the exchange constants within a Heisenberg model, is needed. The latter case can occur by exceeding the Stoner criterion  $\alpha_0 = \rho(E_F)I > 1$ , where  $\rho(E_F)$  is the density of electronic states at the Fermi energy and  $I$  is the effective Coulomb repulsion [11,21,22]. Here, we address which phenomenon is operable in CaCo<sub>2-y</sub>As<sub>2</sub> and present a compelling example of Stoner ferromagnetism in the presence of extreme frustration. Our INS and  $\chi$  data reveal the complete elimination of the fluctuating magnetic moment  $\mu_{\text{fluct}}$  at  $x = 0.25$  without any measurable change to the magnetic frustration. Our density functional theory (DFT) calculations establish that Fe substitution dopes holes into the system and shifts  $E_F$  away from a flat electronic band that creates a large peak in  $\rho(E)$  [18,23]. We conclude that a Stoner-type transition is induced by hole doping.

\*bgueland@ameslab.gov

†Present address: Condensed Matter Physics and Materials Science Division, Brookhaven National Laboratory, Upton, New York 11973, USA.

‡Present address: Institute for Quantum Materials and Technologies, Karlsruhe Institute of Technology, 76021 Karlsruhe, Germany.

§rmcqueen@ameslab.gov

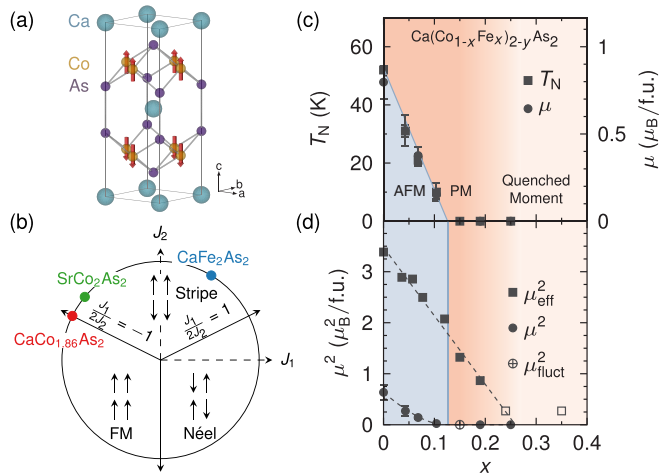


FIG. 1. (a) The unit cell (space group  $I_m^4mm$ ) of CaCo<sub>1.86</sub>As<sub>2</sub> with its A-type antiferromagnetic (AFM) structure shown by red arrows;  $a = b = 3.9906(1)$  Å and  $c = 10.280(1)$  Å at  $T = 300$  K [12,13]. (b) Phase diagram for the  $J_1$ - $J_2$  Heisenberg model on a square lattice. FM corresponds to the A-type order of CaCo<sub>1.86</sub>As<sub>2</sub>. (c) Magnetic phase diagram for Ca(Co<sub>1-x</sub>Fe<sub>x</sub>)<sub>2-y</sub>As<sub>2</sub> [20] showing the Néel temperature  $T_N$  and ordered magnetic moment  $\mu$  vs  $x$ . PM is paramagnetic. The “quenched moment” region has neither static nor dynamic spin correlations. (d) Plots of the  $x$  dependence of  $\mu^2$ , the square of the fluctuating moment  $\mu_{\text{fluct}}^2$ , and the square of the effective moment  $\mu_{\text{eff}}^2$ .  $\mu_{\text{eff}}^2$  for  $x = 0$  is from Ref. [19]. Open squares indicate values for which the modified Curie-Weiss fits used to determine  $\mu_{\text{eff}}^2$  are not valid [17]. Lines are guides to the eye.

Without getting into the microscopic details of the exchange pathways, which is a subject of some debate, we note that the the  $J_1$ - $J_2$  Heisenberg model for a square lattice, with exchange constants  $J_1$  and  $J_2$  between nearest-neighbor (NN) and next-nearest-neighbor spins, respectively, has been used for many 122 pnictides [17,24]. This includes CaCo<sub>1.86</sub>As<sub>2</sub> [8] where the effective exchange-interaction strength between transition metal layers is much weaker than the effective interactions within the planes [8].

Within this model, the quasi-1D spin fluctuations in CaCo<sub>1.86</sub>As<sub>2</sub> give the ratio  $\eta = J_1/(2J_2) = -1.03(2) \approx -1$  [8]. This indicates extreme frustration because it locates the compound at the border between the FM and stripe-AFM phases in Fig. 1(b). CaFe<sub>2</sub>As<sub>2</sub>, on the other hand, lies in the stripe region with an AFM  $J_1$  and exhibits stripe-AFM order [7,14], whereas the stripe-AFM spin fluctuations in paramagnetic (PM) SrCo<sub>2</sub>As<sub>2</sub> require a smaller value of  $\eta$ . This suggests that the exchange constants and, hence, magnetic frustration in these cobalt arsenides, are tunable [9,25]. Such tunability, which in principle might be possible by carrier doping, offers the enticing prospect of finding a quantum phase transition [26] and spin-liquid ground states [27,28]. More discussion of the Stoner and  $J_1$ - $J_2$  models is given in the Supplemental Material (SM) [17].

In this respect, it is interesting to study the evolution of the spin fluctuation spectrum of Ca(Co<sub>1-x</sub>Fe<sub>x</sub>)<sub>2-y</sub>As<sub>2</sub> since Fe substitution (nominal hole doping) suppresses magnetic order by sending both  $T_N$  and  $\mu \rightarrow 0$  at  $x = 0.12(1)$  [20]. Further,

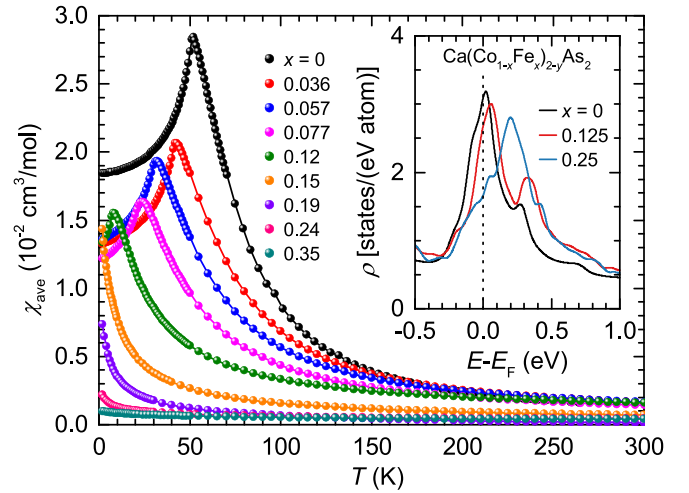


FIG. 2. The powder average of the static magnetic susceptibility  $\chi_{\text{ave}}$  vs  $T$  for various  $x$ . The inset shows the partial electronic density of states per transition metal atom  $\rho$  for  $x = 0, 0.125$ , and  $0.25$  and  $y = 0$ .  $E_F$  is the Fermi energy.

a large body of work on the  $A(\text{Fe}_{1-x}\text{Co}_x)_2\text{As}_2$ ,  $A = \text{Ca}, \text{Sr}, \text{or Ba}$ , high- $T_c$  superconductors and related compounds shows that the ratio of Co to Fe rigidly shifts  $E_F$  albeit with some small level of band broadening due to disorder [1,4,5,29,30]. Thus, a careful study of Ca(Co<sub>1-x</sub>Fe<sub>x</sub>)<sub>2-y</sub>As<sub>2</sub> can address fundamental questions regarding the origin of its collective magnetism and whether critical compositions lead to strong quantum fluctuations and novel properties.

Platelike single crystals of Ca(Co<sub>1-x</sub>Fe<sub>x</sub>)<sub>2-y</sub>As<sub>2</sub> were solution grown using Sn flux and their compositions were measured using energy-dispersive x-ray spectroscopy. INS data were collected at  $T = 5.5$  K for a 2.1-g coaligned single-crystal sample of Ca(Co<sub>0.85</sub>Fe<sub>0.15</sub>)<sub>2</sub>As<sub>2</sub> using the MERLIN spectrometer at the ISIS Neutron and Muon Source at the Rutherford Appleton Laboratory [31]. Measurements were made with  $\mathbf{c}$  fixed parallel to the incident neutron beam which links the  $L$  reciprocal lattice direction to  $E$ .  $\chi(T)$  was determined using using a Quantum Design superconducting quantum interference device (SQUID) magnetometer. The powder average of  $\chi$  [ $\chi_{\text{ave}} = (2/3)\chi_{ab} + (1/3)\chi_c$ ] was found by measuring  $\chi$  perpendicular ( $\chi_{ab}$ ) and parallel ( $\chi_c$ ) to  $\mathbf{c}$ . DFT calculations were performed using the full-potential linear-augmented-plane-wave (FP-LAPW) method [32] with the generalized gradient approximation (GGA) [33]. Further details are given in the SM [17]. Potential effects of chemical disorder on the magnetic order are discussed in Ref. [20]. Since Ca(Co<sub>1-x</sub>Fe<sub>x</sub>)<sub>2-y</sub>As<sub>2</sub> exists in the collapsed-tetragonal phase for  $x \lesssim 0.5$  [20,34–36], and CaFe<sub>2</sub>As<sub>2</sub> is nonmagnetic in the collapsed-tetragonal phase [37–39], we expect Fe to be nonmagnetic for the values of  $x$  studied here.

We begin the presentation of our results by showing the overall suppression of  $\chi(T)$  with increasing  $x$  in Fig. 2. Peaks occur in  $\chi$  near  $T_N$  for samples exhibiting A-type AFM order. We quantify the suppression of  $\chi$  with  $x$  by determining the effective magnetic moment  $\mu_{\text{eff}}(x)$  per formula unit through fitting a modified Curie-Weiss law to  $\chi_{\text{ave}}^{-1}(T)$  as shown in

the SM [17,40,41]. Figure 1(d) shows that  $\mu_{\text{eff}}^2$  decreases with increasing  $x$ , remaining finite across the  $T = 0$  K AFM-PM transition. Whereas the Curie-Weiss law is generally valid for well-localized spins, the self-consistent renormalization theory for itinerant magnetism, which extends Stoner theory, shows that correlated spin fluctuations can drive Curie-Weiss-like behavior at high  $T$  [10,21,22]. As shown in the SM, the Rhodes-Wohlfarth ratio [42] calculated from our data is 1.5–3 which indicates itinerant magnetism [17]. The SM also presents an analysis using Takahashi's theory for itinerant magnets [17].

We next relate  $\chi$  to the electronic structure by plotting the partial  $\rho(E)$  contributed by the Co and Fe orbitals for  $x = 0, 0.125, \text{ and } 0.25$  and  $y = 0$  in the inset of Fig. 2. The total and partial  $\rho(E)$  for  $x = 0$  and  $y = 0$  are given in the SM [17]. A large peak crosses  $E_F$  which has contributions from a flat band with Co  $d_{x^2-y^2}$  orbital character. The flat band's density of states drives Stoner FM when  $\alpha_0 > 1$ . This is supported by work showing that the absence of magnetic order in  $\text{ACo}_2\text{As}_2$ ,  $A = \text{Sr}$  and  $\text{Ba}$ , is a consequence of the flat band lying above  $E_F$  [18]. Our DFT calculations indicate an almost rigid shift in  $E_F$  with increasing hole doping  $x$  with some broadening of the peak in  $\rho(E)$  due to the disorder introduced by substituting Fe for Co. Thus, increasing  $x$  pushes  $E_F$  below the flat band and decreases  $\rho(E_F)$ . Taken together, our  $\chi(T, x)$  and DFT results point to a Stoner-type transition where  $x$  tunes  $\alpha_0$ . When  $\alpha_0 < 1$ ,  $\mu$  vanishes and the continued decrease in  $\mu_{\text{eff}}$  with increasing  $x$  indicates that  $\mu_{\text{fluct}}$  is also strongly suppressed. INS can verify this hypothesis by measuring the spin fluctuations throughout the Brillouin zone.

Constant-energy slices of the INS cross section  $S(\mathbf{Q}, E)$  in the  $(HK)$  plane for  $x = 0.15$  are presented in Figs. 3(a) and 3(b). Figures 3(c) and 3(d) show the data plotted as the imaginary part of the dynamical magnetic susceptibility  $\chi''(\mathbf{Q}, E)$  after subtracting off an isotropic and nonmagnetic background estimated from the main data set and averaging over symmetry-equivalent quadrants of the  $(HK)$  plane. (See the SM [17] and Ref. [43] for more details.) The arrows in Fig. 3(d) indicate the transverse (TR)  $[HH]$  and longitudinal (LO)  $[-KK]$  directions.

Similar to data for  $x = 0$  [8], magnetic scattering in Figs. 3(a)–3(d) extends longitudinally from  $(0,0)$  and is much sharper in the TR direction. Previous INS data for cobalt arsenides demonstrate weak magnetic intensities due to the combination of a small  $\mu_{\text{fluct}}$  and a large energy scale [8,9,25,44]. By normalizing  $S(\mathbf{Q}, E)$  for  $x = 0$  and 0.15 by the mass of the sample used, we find that the magnetic scattering is 100 times weaker for  $x = 0.15$  than for  $x = 0$  and is close to the limit of detection.

Figure 3(e) shows  $\chi''$  in the  $E$ - $[HH]$  plane for incremental integration ranges along the LO direction.  $\chi''(E)$  is steep and extends past 90 meV, which is characteristic of itinerant magnetism [21]. Figures 4(a) and 4(b) show cuts of  $\chi''$  for the TR and LO directions, respectively, for different  $E$ . The TR width of  $\chi''$  is only slightly wider than the calculated experimental resolution [17] and slightly broadens with increasing  $E$ . For the LO direction,  $\chi''$  is practically constant with increasing  $Q$  for a given  $E$  and exhibits an overall change in magnitude consistent with the  $\chi''(E)$  cut in Fig. 4(c).

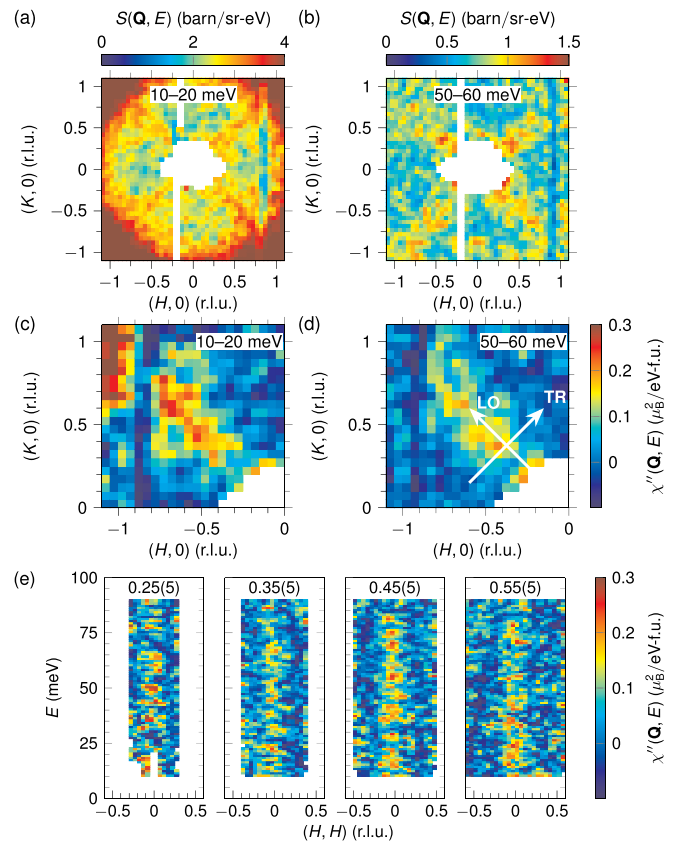


FIG. 3. (a), (b) Slices of the INS cross section  $S(\mathbf{Q}, E)$  in the  $(HK)$  plane at  $T = 5.5$  K integrated over (a)  $E = 10\text{--}20$  meV and (b)  $50\text{--}60$  meV. (c), (d) Data corresponding to (a) and (b), respectively, plotted as  $\chi''(\mathbf{Q}, E)$  after an isotropic background subtraction [17] and averaging over symmetry-equivalent quadrants of the  $(HK)$  plane. Data in (a) and (c) [(b) and (d)] are for  $E_i = 75$  meV (125 meV). The transverse (TR)  $[HH]$  and longitudinal (LO)  $[-KK]$  directions are indicated in (d). (e) TR slices of  $E_i = 125$  meV data corresponding to (d). TR slices for  $E_i = 75$  meV are shown in the SM [17]. From left to right, plots are for integration ranges of  $(-K, K) = (-0.25 \pm 0.05, 0.25 \pm 0.05)$ ,  $(-0.35 \pm 0.05, 0.35 \pm 0.05)$ ,  $(-0.45 \pm 0.05, 0.45 \pm 0.05)$ , and  $(-0.55 \pm 0.05, 0.55 \pm 0.05)$  r.l.u.

The cut in Fig. 4(c) is for integration ranges of  $(H, H) = -0.1$  to  $0.1$  r.l.u. and  $(-K, K) = 0.2\text{--}0.7$  r.l.u.  $\chi''(E)$  peaks around 20 meV and diminishes with increasing  $E$ . The dip at  $\approx 25$  meV comes from errors in the background subtraction due to strong contamination by Al phonons. The lack of periodic variations in  $\chi''(E)$  indicates practically zero dispersion along  $\mathbf{L}$ . Summarizing, other than the much lower intensity, which is consistent with the suppression of  $\chi$  in Fig. 2, the INS data for  $x = 0.15$  are similar to those for  $x = 0$  [8], showing quasi-1D spin fluctuations.

Magnetic fluctuations in the PM, AFM, and superconducting phases of various 122 pnictides have been described by a diffusive model for 2D spin fluctuations in a nearly AFM or nearly FM Fermi liquid [21] using the  $J_1$ - $J_2$  Heisenberg model for exchange within the transition metal planes [7–9,24,43,45–47]. Within a random-phase

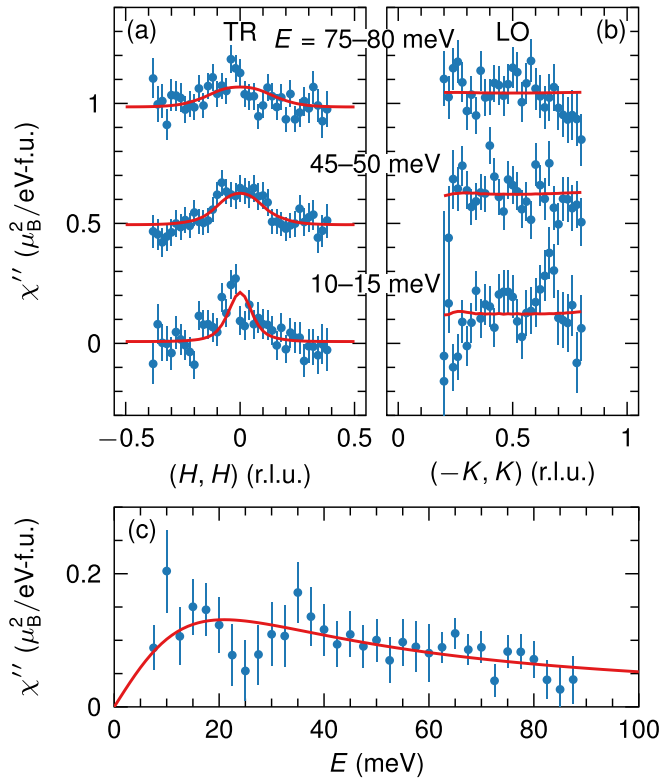


FIG. 4. (a) Transverse (TR) (left) and (b) longitudinal (LO) (right) cuts of  $\chi''(\mathbf{Q}, E)$  at  $T = 5.5$  K for values of  $E$  corresponding to  $L \approx 1, 3$ , and  $5$  r.l.u. TR (LO) cuts are integrated over  $0.2-0.7$  r.l.u. ( $-0.1$  to  $0.1$  r.l.u.) in the LO (TR) direction. Data sets are offset by  $0.5\mu_B^2/\text{eV f.u.}$  Data for  $E = 10-15$  meV ( $E \geq 45$  meV) are for  $E_i = 75$  meV (125 meV). (c)  $\chi''(E)$  at  $T = 5.5$  K from integrating over  $-0.1$  to  $0.1$  r.l.u. ( $0.2-0.7$  r.l.u.) along the TR (LO) direction. The  $E = 7.5$  meV point is from  $E_i = 75$  meV data, points between  $10$  and  $60$  meV are the average of  $E_i = 75$  and  $125$  meV data, and  $E > 60$  meV data correspond to  $E_i = 125$  meV. An isotropic background subtraction has been performed [17] and data were averaged over symmetry-equivalent quadrants of the  $(HK)$  plane. Lines are the results of fits described in the text.

approximation, the model gives

$$\chi''(\mathbf{Q}, E) = \frac{\chi'(\mathbf{Q}_\tau, 0)\Gamma E}{\Gamma^2\{1 + \frac{4\xi^2}{a^2}[\eta(c_+ + c_-) + c_+c_- - 2\eta - 1]\}^2 + E^2}. \quad (1)$$

Here,  $\chi'(\mathbf{Q}_\tau, 0)$  is the staggered static susceptibility at  $\mathbf{Q}_\tau$ ,  $\xi$  is the magnetic correlation length,  $\Gamma$  quantifies damping of the fluctuations,  $c_\pm = \cos[(q_x \pm q_y)a/2]$ , where  $x$  and  $y$  denote perpendicular directions connecting NN spins, and  $\mathbf{q} = \mathbf{Q} - \mathbf{Q}_\tau$ .  $\mathbf{Q}_\tau$  is a reciprocal-lattice position corresponding to the magnetic propagation vector  $\tau$ . For our case,  $\tau = (0, 0)$ .

We simultaneously fit Eq. (1) to TR, LO, and  $E$  cuts of the INS data but found that the value for  $\Gamma$  had too much uncertainty. To mitigate this, we fit the data in Fig. 4(c) using the typical quasielastic diffuse magnetic scattering form of  $\chi''(E) = AE/(\Gamma^2 + E^2)$ , where  $A$  is a scale factor [48]. We next simultaneously fit TR and LO cuts taken every 5 meV to Eq. (1) while keeping  $\Gamma$  fixed. Lines in Fig. 4 show examples of the fits with  $\chi'(\mathbf{Q}_\tau, 0) = 3.4(3) \times 10^{-4} \mu_B^2/\text{meV f.u.}$ ,

$\xi/a = 1.01(8)$ ,  $\Gamma = 21(3)$  meV, and  $\eta = -0.97(1)$ . Simulated slices of  $\chi''(\mathbf{Q}, E)$  are shown in the SM [17].

With the exception of the extraordinarily small value of  $\chi'(\mathbf{Q}_\tau, 0)$ , which is consistent with the  $\chi(T)$  data, the determined parameters are analogous to those for  $x = 0$ . Thus, our fits find a similar level of frustration exists for  $x = 0$  and  $0.15$  since  $\eta \approx -1$  for both compositions. A table listing the fitted parameters for  $x = 0$  and  $0.15$  and for other 122 pnictides is given in the SM [17]. The INS data can also be used to determine  $\mu_{\text{fluct}}$  by integrating  $\chi''$  over  $\mathbf{Q}$  and  $E$  [17]. We find an extraordinarily small value of  $\mu_{\text{fluct}} = 0.09(1)\mu_B/\text{f.u.}$  for  $x = 0.15$ , which is 10–100 times smaller than  $\mu_{\text{fluct}}$  for related compounds [17].

As noted above, even though  $\chi'(\mathbf{Q}_\tau, 0)$  for  $x = 0$  has yet to be measured on an absolute scale, we know that  $S(\mathbf{Q}, E)$  is  $\approx 100$  times stronger for  $x = 0$  than for  $x = 0.15$  [8]. Thus,  $\mu_{\text{fluct}}$  substantially decreases with increasing  $x$ . Taken together with the decrease in  $\mu_{\text{eff}}$  and the elimination of  $\mu$  with increasing  $x$ , the exceedingly small value of  $\mu_{\text{fluct}}$  for  $x = 0.15$  indicates that hole doping weakens the spin correlations associated with the A-type order. However, since  $\eta \approx 1$  for both  $x = 0$  and  $0.15$ , the weakening is not due to modifying the degree of frustration. Rather, taking into account the decrease in  $\mu$  and  $\mu_{\text{fluct}}$  with increasing  $x$  and extrapolating the decrease in  $\mu_{\text{eff}}^2$  with  $x$  in Fig. 1(d) indicates elimination of the total magnetic moment at  $x \approx 0.25$ .

Since ferromagnetism within the Co planes dominates the magnetic energy scale [8] and our DFT results indicate that hole doping shifts  $E_F$  away from a peak in  $\rho(E)$ , the quenching of the moment can be explained in terms of a Stoner transition: A decrease in  $\rho(E_F)$  lowers  $\alpha_0 = \rho(E_F)I$  below 1 at  $x = 0.12$  and eliminates the FM order within the Co planes and, in turn, the A-type order. As evidenced by the further decrease in  $\mu_{\text{eff}}$  and  $\mu_{\text{fluct}}$ , more hole doping eventually completely destroys FM correlations within the Co planes which results in a quenched moment for  $x \approx 0.25$ .

Quenching of the total moment has also been observed for  $\text{CaFe}_2\text{As}_2$  which exhibits stripe-AFM order. However, in this case the quenching accompanies a pressure-induced first-order structural phase transition into the collapsed tetragonal (cT) phase characterized by  $c/a \lesssim 2.8$  [37,38,49]. The Fermi surface in the ambient-pressure uncollapsed phase exhibits features consistent with nesting which are not present in the cT phase [50,51] and DFT calculations indicate that there disappearance is not due to a rigid shift in  $E_F$  [50].  $\text{Ca}(\text{Co}_{1-x}\text{Fe}_x)_{2-y}\text{As}_2$ , on the other hand, crosses over to the cT phase at  $x \approx 0.5$  [20], well past  $x = 0.25$ .

Finally, a Stoner transition is a quantum phase transition (QPT) since it occurs at  $T = 0$  K [10,26]. Indeed, the heat capacity data for  $x = 0.15$  shown in the SM [17] indicate that non-Fermi-liquid behavior occurs below  $\approx 10$  K which is attributed to a QPT similar to previous reports for  $\text{Ni}_x\text{Pd}_{1-x}$  [52] and  $\text{YFe}_2\text{Al}_{10}$  [53]. QPTs in clean itinerant FM are expected to be first order [26], however, the magnetic transitions in  $\text{Ca}(\text{Co}_{1-x}\text{Fe}_x)_{2-y}\text{As}_2$  appear continuous [20]. Disorder caused, for example, by Fe substitution and Co vacancies can drive a continuous QPT. On the other hand, even though the FM Co planes dominate the magnetic energy, A-type AFM order is present. These considerations give compelling reasons to look for quantum fluctuations in other values of  $x$ , particularly those around  $x = 0.12$  and  $0.25$ .

Summarizing, we report the observation of quenching of a magnetic moment by a Stoner-type transition. Our results indicate that in addition to the loss of A-type AFM order at  $x = 0.12$ , increasing  $x$  eliminates the remaining FM spin correlations in  $\text{Ca}(\text{Co}_{1-x}\text{Fe}_x)_{2-y}\text{As}_2$  by  $x \approx 0.25$  while maintaining extreme frustration. Our DFT calculations show that increasing  $x$  results in hole doping that rigidly shifts  $E_F$  away from a peak in  $\rho(E)$  from a flat conduction band. Future investigations looking for more evidence of a QPT for  $x$  spanning the disappearance of AFM order and the quenching of the moment should be insightful.

We are grateful for conversations with H. C. Walker, A. I. Goldman, A. Kreyssig, P. P. Orth, and D. Vaknin, and to D. L. Schlögl for assistance with coaligning single crystals. Work at the Ames Laboratory was supported by the U.S. Department of Energy (DOE), Basic Energy Sciences, Division of Materials Sciences & Engineering, under Contract No. DE-AC02-07CH11358. Experiments at the ISIS Neutron and Muon Source were supported by a beamtime allocation RB1810596 from the Science and Technology Facilities Council.

- 
- [1] N. S. Sangeetha, L.-L. Wang, A. V. Smirnov, V. Smetana, A.-V. Mudring, D. D. Johnson, M. A. Tanatar, R. Prozorov, and D. C. Johnston, Non-Fermi-liquid types of behavior associated with a magnetic quantum critical point in  $\text{Sr}(\text{Co}_{1-x}\text{Ni}_x)_2\text{As}_2$  single crystals, *Phys. Rev. B* **100**, 094447 (2019).
- [2] S. Pakhira, N. S. Sangeetha, V. Smetana, A.-V. Mudring, and D. C. Johnston, Ferromagnetic cluster-glass phase in  $\text{Ca}(\text{Co}_{1-x}\text{Ir}_x)_{2-y}\text{As}_2$  crystals, *Phys. Rev. B* **102**, 024410 (2020).
- [3] R. M. Fernandes, A. V. Chubukov, J. Knolle, I. Eremin, and J. Schmalian, Preemptive nematic order, pseudogap, and orbital order in the iron pnictides, *Phys. Rev. B* **85**, 024534 (2012).
- [4] D. C. Johnston, The puzzle of high temperature superconductivity in layered iron pnictides and chalcogenides, *Adv. Phys.* **59**, 803 (2010).
- [5] P. C. Canfield and S. L. Bud'ko, FeAs-based superconductivity: A case study of the effects of transition metal doping on  $\text{BaFe}_2\text{As}_2$ , *Annu. Rev. Condens. Matter Phys.* **1**, 27 (2010).
- [6] G. R. Stewart, Superconductivity in iron compounds, *Rev. Mod. Phys.* **83**, 1589 (2011).
- [7] S. O. Diallo, D. K. Pratt, R. M. Fernandes, W. Tian, J. L. Zarestky, M. Lumsden, T. G. Perring, C. L. Broholm, N. Ni, S. L. Bud'ko, P. C. Canfield, H.-F. Li, D. Vaknin, A. Kreyssig, A. I. Goldman, and R. J. McQueeney, Paramagnetic spin correlations in  $\text{CaFe}_2\text{As}_2$  single crystals, *Phys. Rev. B* **81**, 214407 (2010).
- [8] A. Sapkota, B. G. Ueland, V. K. Anand, N. S. Sangeetha, D. L. Abernathy, M. B. Stone, J. L. Niedziela, D. C. Johnston, A. Kreyssig, A. I. Goldman, and R. J. McQueeney, Effective One-Dimensional Coupling in the Highly Frustrated Square-Lattice Itinerant Magnet  $\text{CaCo}_{2-y}\text{As}_2$ , *Phys. Rev. Lett.* **119**, 147201 (2017).
- [9] W. Jayasekara, Y. Lee, A. Pandey, G. S. Tucker, A. Sapkota, J. Lamsal, S. Calder, D. L. Abernathy, J. L. Niedziela, B. N. Harmon, A. Kreyssig, D. Vaknin, D. C. Johnston, A. I. Goldman, and R. J. McQueeney, Stripe Antiferromagnetic Spin Fluctuations in  $\text{SrCo}_2\text{As}_2$ , *Phys. Rev. Lett.* **111**, 157001 (2013).
- [10] J. M. Santiago, C.-L. Huang, and E. Morosan, Itinerant magnetic metals, *J. Condens. Matter Phys.* **29**, 373002 (2017).
- [11] E. C. Stoner, Collective electron ferromagnetism, *Proc. R. Soc. London, Ser. A* **165**, 372 (1938).
- [12] D. G. Quirinale, V. K. Anand, M. G. Kim, A. Pandey, A. Huq, P. W. Stephens, T. W. Heitmann, A. Kreyssig, R. J. McQueeney, D. C. Johnston, and A. I. Goldman, Crystal and magnetic structure of  $\text{CaCo}_{1.86}\text{As}_2$  studied by x-ray and neutron diffraction, *Phys. Rev. B* **88**, 174420 (2013).
- [13] K. Momma and F. Izumi, VESTA: A three-dimensional visualization system for electronic and structural analysis, *J. Appl. Crystallogr.* **41**, 653 (2008).
- [14] S. O. Diallo, V. P. Antropov, T. G. Perring, C. Broholm, J. J. Pulikkotil, N. Ni, S. L. Bud'ko, P. C. Canfield, A. Kreyssig, A. I. Goldman, and R. J. McQueeney, Itinerant Magnetic Excitations in Antiferromagnetic  $\text{CaFe}_2\text{As}_2$ , *Phys. Rev. Lett.* **102**, 187206 (2009).
- [15] L. Harnagea, S. Singh, G. Friemel, N. Leps, D. Bombor, M. Abdel-Hafiez, A. U. B. Wolter, C. Hess, R. Klingeler, G. Behr, S. Wurmehl, and B. Büchner, Phase diagram of the iron arsenide superconductors  $\text{Ca}(\text{Fe}_{1-x}\text{Co}_x)_2\text{As}_2$  ( $0 \leq x \leq 0.2$ ), *Phys. Rev. B* **83**, 094523 (2011).
- [16] R. Hu, S. Ran, W. E. Straszheim, S. L. Bud'ko, and P. C. Canfield, Single crystal growth and superconductivity of  $\text{Ca}(\text{Fe}_{1-x}\text{Co}_x)_2\text{As}_2$ , *Philos. Mag.* **92**, 3113 (2012).
- [17] See Supplemental Material at <http://link.aps.org/supplemental/10.1103/PhysRevB.104.L220410> for further details of the static magnetic susceptibility and inelastic neutron scattering measurements, and the density functional theory calculations, as well as low-temperature heat capacity data for  $x = 0.15$ .
- [18] H. Mao and Z. Yin, Electronic structure and spin dynamics of  $\text{ACo}_2\text{As}_2$  ( $A = \text{Ba}, \text{Sr}, \text{Ca}$ ), *Phys. Rev. B* **98**, 115128 (2018).
- [19] V. K. Anand, R. S. Dhaka, Y. Lee, B. N. Harmon, A. Kaminski, and D. C. Johnston, Physical properties of metallic antiferromagnetic  $\text{CaCo}_{1.86}\text{As}_2$  single crystals, *Phys. Rev. B* **89**, 214409 (2014).
- [20] W. T. Jayasekara, A. Pandey, A. Kreyssig, N. S. Sangeetha, A. Sapkota, K. K. Kothapalli, V. K. Anand, W. Tian, D. Vaknin, D. C. Johnston, R. J. McQueeney, A. I. Goldman, and B. G. Ueland, Suppression of magnetic order in  $\text{CaCo}_{1.86}\text{As}_2$  with Fe substitution: Magnetization, neutron diffraction, and x-ray diffraction studies of  $\text{Ca}(\text{Co}_{1-x}\text{Fe}_x)_y\text{As}_2$ , *Phys. Rev. B* **95**, 064425 (2017).
- [21] T. Moriya, *Spin Fluctuations in Itinerant Electron Magnetism* (Springer, Berlin, 1985).
- [22] Y. Takahashi, *Spin Fluctuation Theory of Itinerant Electron Magnetism*, Springer Tracts in Modern Physics (Springer, Berlin, 2013), Vol. 253.
- [23] H. Tasaki, From Nagaoka's ferromagnetism to flat-band ferromagnetism and beyond: An introduction to ferromagnetism in the Hubbard model, *Prog. Theor. Phys.* **99**, 489 (1998).
- [24] P. Dai, Antiferromagnetic order and spin dynamics in iron-based superconductors, *Rev. Mod. Phys.* **87**, 855 (2015).

- [25] B. Li, B. G. Ueland, W. T. Jayasekara, D. L. Abernathy, N. S. Sangeetha, D. C. Johnston, Q.-P. Ding, Y. Furukawa, P. P. Orth, A. Kreyssig, A. I. Goldman, and R. J. McQueeney, Competing magnetic phases and itinerant magnetic frustration in  $\text{SrCo}_2\text{As}_2$ , *Phys. Rev. B* **100**, 054411 (2019).
- [26] M. Brando, D. Belitz, F. M. Grosche, and T. R. Kirkpatrick, Metallic quantum ferromagnets, *Rev. Mod. Phys.* **88**, 025006 (2016).
- [27] L. Savary and L. Balents, Quantum spin liquids: A review, *Rep. Prog. Phys.* **80**, 016502 (2016).
- [28] Y. Zhou, K. Kanoda, and T.-K. Ng, Quantum spin liquid states, *Rev. Mod. Phys.* **89**, 025003 (2017).
- [29] P. Dai, J. Hu, and E. Dagotto, Magnetism and its microscopic origin in iron-based high-temperature superconductors, *Nat. Phys.* **8**, 709 (2012).
- [30] Y. Li, Z. Liu, Z. Xu, Y. Song, Y. Huang, D. Shen, N. Ma, A. Li, S. Chi, M. Frontzek, H. Cao, Q. Huang, W. Wang, Y. Xie, R. Zhang, Y. Rong, W. A. Shelton, D. P. Young, J. F. DiTusa, and P. Dai, Flat-band magnetism and helical magnetic order in Ni-doped  $\text{SrCo}_2\text{As}_2$ , *Phys. Rev. B* **100**, 094446 (2019).
- [31] R. J. McQueeney, B. G. Ueland, B. Li, A. Sapkota, and T. G. Perring, Exploring magnetic frustration in a square-lattice metallic system: Spin fluctuations in Fe-doped  $\text{CaCo}_2\text{As}_2$ , STFC ISIS Neutron and Muon Source, <https://doi.org/10.5286/ISIS.E.RB1810596>.
- [32] P. Blaha, K. Schwarz, F. Tran, R. Laskowski, G. K. H. Madsen, and L. D. Marks, WIEN2K: An APW+lo program for calculating the properties of solids, *J. Chem. Phys.* **152**, 074101 (2020).
- [33] J. P. Perdew, K. Burke, and M. Ernzerhof, Generalized Gradient Approximation Made Simple, *Phys. Rev. Lett.* **77**, 3865 (1996).
- [34] R. Hoffmann and C. Zheng, Making and breaking bonds in the solid state: The  $\text{ThCr}_2\text{Si}_2$  structure, *J. Phys. Chem. A* **89**, 4175 (1985).
- [35] M. Reehuis and W. Jeitschko, Structure and magnetic properties of the phosphides  $\text{CaCo}_2\text{P}_2$  and  $\text{LnT}_2\text{P}_2$  with  $\text{ThCr}_2\text{Si}_2$  structure and  $\text{LnTP}$  with  $\text{PbFCl}$  structure ( $\text{Ln} = \text{Lanthanoids}$ ,  $T = \text{Fe, Co, Ni}$ ), *J. Phys. Chem. Solids* **51**, 961 (1990).
- [36] M. Reehuis, W. Jeitschko, G. Kotzyba, B. Zimmer, and X. Hu, Antiferromagnetic order in the  $\text{ThCr}_2\text{Si}_2$  type phosphides  $\text{CaCo}_2\text{P}_2$  and  $\text{CeCo}_2\text{P}_2$ , *J. Alloys Compd.* **266**, 54 (1998).
- [37] A. Kreyssig, M. A. Green, Y. Lee, G. D. Samolyuk, P. Zajdel, J. W. Lynn, S. L. Bud'ko, M. S. Torikachvili, N. Ni, S. Nandi, J. B. Leão, S. J. Poulton, D. N. Argyriou, B. N. Harmon, R. J. McQueeney, P. C. Canfield, and A. I. Goldman, Pressure-induced volume-collapsed tetragonal phase of  $\text{CaFe}_2\text{As}_2$  as seen via neutron scattering, *Phys. Rev. B* **78**, 184517 (2008).
- [38] A. I. Goldman, A. Kreyssig, K. Prokeš, D. K. Pratt, D. N. Argyriou, J. W. Lynn, S. Nandi, S. A. J. Kimber, Y. Chen, Y. B. Lee, G. Samolyuk, J. B. Leão, S. J. Poulton, S. L. Bud'ko, N. Ni, P. C. Canfield, B. N. Harmon, and R. J. McQueeney, Lattice collapse and quenching of magnetism in  $\text{CaFe}_2\text{As}_2$  under pressure: A single-crystal neutron and x-ray diffraction investigation, *Phys. Rev. B* **79**, 024513 (2009).
- [39] J. H. Soh, G. S. Tucker, D. K. Pratt, D. L. Abernathy, M. B. Stone, S. Ran, S. L. Bud'ko, P. C. Canfield, A. Kreyssig, R. J. McQueeney, and A. I. Goldman, Inelastic Neutron Scattering Study of a Nonmagnetic Collapsed Tetragonal Phase in Non-superconducting  $\text{CaFe}_2\text{As}_2$ : Evidence of the Impact of Spin Fluctuations on Superconductivity in the Iron-Arsenide Compounds, *Phys. Rev. Lett.* **111**, 227002 (2013).
- [40] C. Kittel, *Introduction to Solid State Physics* (Wiley, New York, 2004).
- [41] N. Ashcroft and N. Mermin, *Solid State Physics* (Cengage Learning, New York, 2020).
- [42] P. Rhodes and E. P. Wohlfarth, The effective Curie-Weiss constant of ferromagnetic metals and alloys, *Proc. R. Soc. London, Ser. A* **273**, 247 (1963).
- [43] G. S. Tucker, Nature of magnetic excitations in the iron pnictides and its pertinence to superconductivity as studied by inelastic neutron scattering, Ph.D. thesis, Iowa State University, 2015.
- [44] Y. Li, Z. Yin, Z. Liu, W. Wang, Z. Xu, Y. Song, L. Tian, Y. Huang, D. Shen, D. L. Abernathy, J. L. Niedziela, R. A. Ewings, T. G. Perring, D. M. Pajerowski, M. Matsuda, P. Bourges, E. Mechthild, Y. Su, and P. Dai, Coexistence of Ferromagnetic and Stripe Antiferromagnetic Spin Fluctuations in  $\text{SrCo}_2\text{As}_2$ , *Phys. Rev. Lett.* **122**, 117204 (2019).
- [45] D. Inosov, J. Park, P. Bourges, D. Sun, Y. Sidis, A. Schneidewind, K. Hradil, D. Haug, C. Lin, B. Keimer, and V. Hinkov, Normal-state spin dynamics and temperature-dependent spin-resonance energy in optimally doped  $\text{BaFe}_{1.85}\text{Co}_{0.15}\text{As}_2$ , *Nat. Phys.* **6**, 178 (2010).
- [46] A. Sapkota, P. Das, A. E. Böhmer, B. G. Ueland, D. L. Abernathy, S. L. Bud'ko, P. C. Canfield, A. Kreyssig, A. I. Goldman, and R. J. McQueeney, Doping evolution of spin fluctuations and their peculiar suppression at low temperatures in  $\text{Ca}(\text{Fe}_{1-x}\text{Co}_x)_2\text{As}_2$ , *Phys. Rev. B* **97**, 174519 (2018).
- [47] G. S. Tucker, R. M. Fernandes, D. K. Pratt, A. Thaler, N. Ni, K. Marty, A. D. Christianson, M. D. Lumsden, B. C. Sales, A. S. Sefat, S. L. Bud'ko, P. C. Canfield, A. Kreyssig, A. I. Goldman, and R. J. McQueeney, Crossover from spin waves to diffusive spin excitations in underdoped  $\text{Ba}(\text{Fe}_{1-x}\text{Co}_x)_2\text{As}_2$ , *Phys. Rev. B* **89**, 180503(R) (2014).
- [48] G. Shirane, S. M. Shapiro, and J. M. Tranquada, *Neutron Scattering with a Triple-Axis Spectrometer: Basic Techniques* (Cambridge University Press, Cambridge, U.K., 2002).
- [49] V. K. Anand, P. K. Perera, A. Pandey, R. J. Goetsch, A. Kreyssig, and D. C. Johnston, Crystal growth and physical properties of  $\text{SrCu}_2\text{As}_2$ ,  $\text{SrCu}_2\text{Sb}_2$ , and  $\text{BaCu}_2\text{Sb}_2$ , *Phys. Rev. B* **85**, 214523 (2012).
- [50] R. S. Dhaka, R. Jiang, S. Ran, S. L. Bud'ko, P. C. Canfield, B. N. Harmon, A. Kaminski, M. Tomić, R. Valentí, and Y. Lee, Dramatic changes in the electronic structure upon transition to the collapsed tetragonal phase in  $\text{CaFe}_2\text{As}_2$ , *Phys. Rev. B* **89**, 020511(R) (2014).
- [51] T. Yildirim, Strong Coupling of the Fe-Spin State and the As-As Hybridization in Iron-Pnictide Superconductors from First-Principle Calculations, *Phys. Rev. Lett.* **102**, 037003 (2009).
- [52] M. Nicklas, M. Brando, G. Knebel, F. Mayr, W. Trinkl, and A. Loidl, Non-Fermi-Liquid Behavior at a Ferromagnetic Quantum Critical Point in  $\text{Ni}_x\text{Pd}_{1-x}$ , *Phys. Rev. Lett.* **82**, 4268 (1999).
- [53] L. S. Wu, M. S. Kim, K. Park, A. M. Tselik, and M. C. Aronson, Quantum critical fluctuations in layered  $\text{YFe}_2\text{Al}_{10}$ , *Proc. Natl. Acad. Sci. USA* **111**, 14088 (2014).